Linear and non-linear magneto-optical studies of Pt/Co/Pt thin films



2001 J. Phys.: Condens. Matter 13 9867

(http://iopscience.iop.org/0953-8984/13/44/304)

INSTITUTE OF PHYSICS PUBLISHING JOURNAL OF PHYSICS: CONDENSED MATTER

J. Phys.: Condens. Matter **13** (2001) 9867–9878 PII: S0953-8984(01)22710-6

# Linear and non-linear magneto-optical studies of Pt/Co/Pt thin films

**V V Pavlov[1,2], J Ferré[2], P Meyer[2], G Tessier[3], P Georges[3], A Brun[3], P Beauvillain[4] and V Mathet[4]**

[1] A F Ioffe Physical Technical Institute of the Russian Academy of Sciences, 194021 St Petersburg, Russia
[2] Laboratoire de Physique des Solides, UMR CNRS 8502, Bâtiment 510, Université de Paris-Sud, 91405 Orsay Cédex, France
[3] Institut d'Optique Théorique et Appliquée, UMR CNRS 8501, Bâtiment 503, Université de Paris-Sud, 91403 Orsay Cédex, France
[4] Institut d'Électronique Fondamentale, UMR CNRS 8622, Bâtiment 220, Université de Paris-Sud, 91405 Orsay Cédex, France

Received 7 March 2001, in final form 17 July 2001
Published 19 October 2001
Online at stacks.iop.org/JPhysCM/13/9867

**Abstract**

Linear magneto-optical Kerr effect (MOKE) microscopy and magnetization-induced second-harmonic-generation (MSHG) magnetometry and imaging were used as two complementary optical techniques to measure the magnetic hysteresis loops and to visualize the domain structure in Pt/Co/Pt thin films with a weak uniaxial in-plane magnetic anisotropy. While the MOKE is used to probe the magnetization over the full thickness of the Co layer, MSHG is used to check the Co/Pt interfaces selectively. When the magnetic field $\boldsymbol{H}$ is not applied along the easy axis $\boldsymbol{a}$, longitudinal MOKE and MSHG hysteresis loops exhibit different shapes. The differences between the longitudinal MOKE and MSHG magnetic pattern images for $\boldsymbol{H} \parallel \boldsymbol{a}$ are only found in domain wall regions. All of these results are interpreted by considering transverse components of the non-linear optical polarization.

## 1. Introduction

Since the first synthesis of Pt/Co/Pt multilayers [1] it has been demonstrated that these thin-film structures have great potential for magnetic and magneto-optical (MO) applications. Pt/Co/Pt multilayers are promising for high-density rewritable MO storage usage because of their enhanced MO response in the blue spectral region and the squareness of their magnetic hysteresis loops [2, 3]. For specific magnetic devices, the processes governing the magnetization reversal in such films play an important role. In order to get complete information on the mechanisms involved, a good knowledge of the magnetization state in

  

the bulk and at interfaces is required. In the electric dipole approximation, optical second-harmonic generation (SHG) by centrosymmetric materials is only allowed at free surfaces and buried interfaces due to the breaking of the space-inversion symmetry. For the same reason, magnetization-induced second-harmonic generation (MSHG) has been proven to be selectively sensitive to the magnetization states of surfaces and interfaces of ultrathin-film structures [4]. Thus, the magnetization states of buried interfaces can be checked by means of MSHG, whereas traditional optical methods, such as reflection or linear magneto-optical Kerr effect (MOKE) microscopy, probe the film structure over the penetration depth of the light. Note that SHG imaging has also been used as an effective tool to visualize ferroelectric and magnetic domain structures in non-centrosymmetric bulk materials [5, 6]. Due to its high MO contrast, MSHG microscopy has already been used as a technique complementary to MOKE imaging for visualization of the magnetic configuration at interfaces of CoNi/Pt thin-film structures [7]. Near-field MSHG microscopy has also been successfully applied to investigate some surface domain structures [8,9]. In the case of antiferromagnetically ordered crystals, SHG imaging gives a unique way to reveal antiferromagnetic spin structures [10].

In this work, a Pt/Co/Pt metallic ultrathin-film structure, prepared by slow evaporation of Pt and Co metals in a high-vacuum chamber [11], was studied by combining linear MOKE and non-linear MSHG magnetometry and microscopy. Direct comparisons between MOKE and MSHG hysteresis loops and imaging of the magnetic domain patterns are presented. The corresponding hysteresis loops can be significantly different in shape while the domain wall structure may be better revealed by MSHG imaging than by MOKE microscopy.

## 2. Principles of measurements

### *2.1. Non-linear polarization and SHG intensity*

Non-linear polarization, $\boldsymbol{P}(2\omega)$, can be excited during the interaction of intense optical radiation with a medium. In the electric dipole approximation it can be written as [12]

$$\boldsymbol{P}(2\omega) = \varepsilon_0 \hat{\boldsymbol{\chi}}^{(2)} \boldsymbol{E}(\omega)\boldsymbol{E}(\omega) \tag{1}$$

where $\boldsymbol{E}(\omega)$ is the optical electric field at the fundamental frequency, $\hat{\boldsymbol{\chi}}^{(2)}$ being the non-linear susceptibility tensor. In the case of a magnetic medium, the non-linear polarization has an additional contribution:

$$\boldsymbol{P}^{mag}(2\omega) = \mathrm{i}\varepsilon_0 \hat{\boldsymbol{\chi}}^{(3)} \boldsymbol{E}(\omega)\boldsymbol{E}(\omega)\boldsymbol{M}(0) \tag{2}$$

where $\boldsymbol{M}(0)$ is the quasi-static sample magnetization. In equations (1) and (2) the $\hat{\boldsymbol{\chi}}^{(2)}$ tensors and $\hat{\boldsymbol{\chi}}^{(3)}$ are only allowed in a non-centrosymmetric medium. Furthermore, their non-vanishing components depend on the crystallographic symmetry. Superposition of the two electromagnetic waves associated with the crystallographic and magnetic contributions described by equations (1) and (2) gives rise to an interference MSHG term linear in magnetization with the intensity

$$I(2\omega, \pm M) \propto \left[ \left|\chi^{(2)}\right|^2 + \left|\chi^{(3)} M\right|^2 \pm 2 \left|\chi^{(2)}\right| \left|\chi^{(3)}\right| M \cos\delta \right] E^4(\omega) \tag{3}$$

where $\delta$ is the phase shift between the optical waves. The signs $+/-$ correspond to the two opposite directions of the magnetization.

For a magnetic layer structure built with structurally centrosymmetric thin films, the contributions to the non-linear polarization arise from the film surface and interfaces, i.e. for every space-inversion symmetry breaking. In the case of a Pt/Co/Pt thin-film structure grown on sapphire, one expects SHG signals from the Pt surface and the Pt/Co and Pt/substrate interfaces.

This phenomenological approach can be successfully used to provide a qualitative description of the SHG data. In order to get quantitative information on non-linear susceptibilities of buried interfaces, a detailed experimental study of the variation of the SHG with the angle of incidence of the light beam at the medium surface is required and can be analysed within a Green function approach [13, 14]. In the present study, we restrict ourselves to comparison of magnetic hysteresis loops and images of domain structures obtained by means of linear and non-linear magneto-optics.

### *2.2. Experimental set-up and samples*

The experimental set-up used for the MOKE and MSHG studies is shown schematically in figure 1. For the SHG experiments a mode-locked Ti:sapphire laser pumped by an Ar laser is used as a source of 100 fs light pulses with a repetition rate of 86 MHz at a wavelength of 800 nm. The light beam is first polarized by means of a Glan polarizer and then focused by a lens on the sample to a spot diameter of about 30 $\mu$m. The average light power arriving on the sample is estimated to be 30 mW. A Babinet-Soleil compensator is used as a half-wave plate to control the polarization of the incident light. The fundamental and SHG light can be P-polarized (TM mode) or S-polarized (TE mode). Proper filtering of the SHG signals is achieved by making an appropriate choice of filters. The RG715 filter is used to eliminate SHG stray light generated by the optical elements placed in front of the sample. Behind the sample, a BG40 filter blocks the light at the fundamental frequency. Due to the very low efficiency of the non-linear process, the SHG light intensity generated by the Pt/Co/Pt film is measured using a high-sensitivity nitrogen-cooled CCD camera. The sample is placed on a rotatable (around the $z$-axis) holder controlled by a stepping motor, providing the possibility to measure the rotational anisotropy of the emerging SHG light. The Pt/Co/Pt film can be

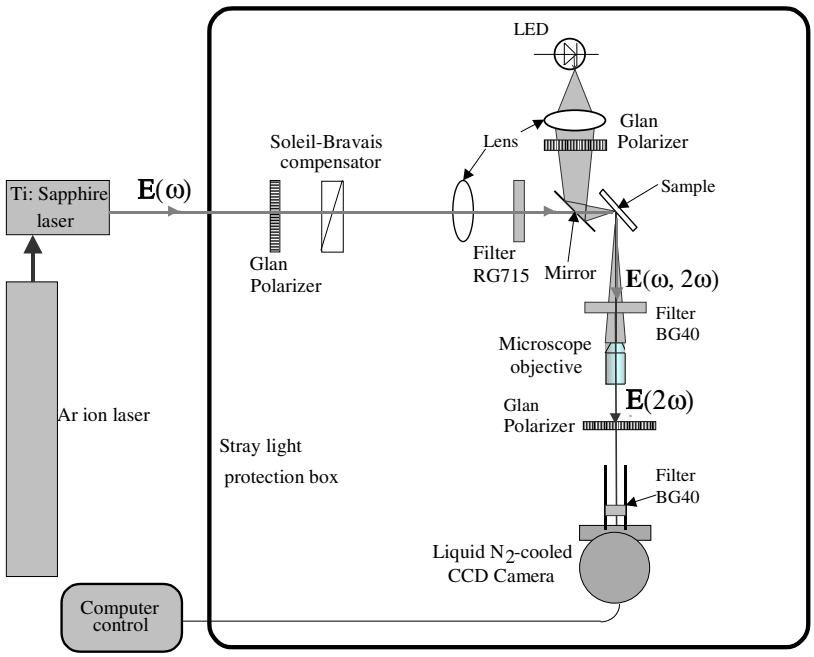


**Figure 1.** A schematic diagram of the MO experimental set-up.

in-plane magnetized by an electromagnet up to a magnetic field of 2 kOe. For the MOKE and MSHG microscopy experiments, the sample was placed on a translation table driven by two high-precision stepping motors in the $x$- and $y$-directions (figure 2). The whole set-up is computer controlled.

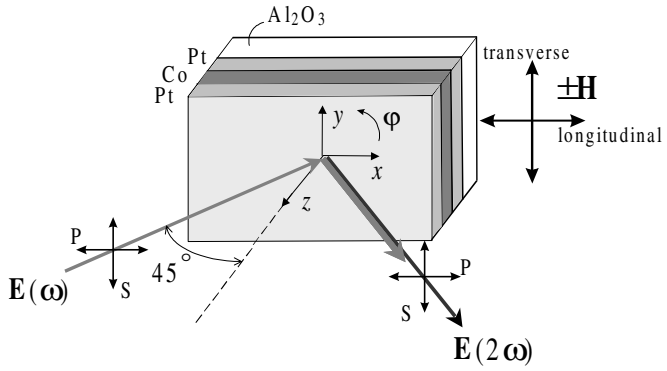


**Figure 2.** The optical configuration used for the MOKE and SHG measurements.

The optical elements used in the MOKE set-up are set as follows (see figure 1). A 2 mW blue LED, emitting at a wavelength of 450 nm, is used as a continuous light source. The light beam is transmitted through a Glan polarizer, then reflected by a removable mirror and focused onto the sample. The optical part of the MOKE set-up placed behind the sample is similar to that used in MSHG experiments. Special attention is paid to the intensity stabilization of the LED and temperature control of the set-up. In this way, it is possible to measure MOKE hysteresis loops in the longitudinal configuration without using an optical modulation technique. In our experiments, the analyser angle $\alpha$ is set at 85° ($\alpha = 0°$ means P-polarization). MOKE and MSHG experiments are performed in light reflected at an angle of incidence of 45°. After passing through the microscope objective and the Glan analyser, the intensity of the reflected beam is measured by means of the same cooled CCD camera. With this experimental set-up, it is then possible to get a precise $x$–$y$ correlated topographic mapping of the MOKE and MSHG signals. This is required for an accurate comparison between data obtained by these two MO methods. We will use the term 'longitudinal configuration' for the situation where the external magnetic field is applied along the $x$-direction in the plane of incidence. The 'transverse configuration' will correspond to the case where $\boldsymbol{H}$ is applied perpendicularly to the plane of incidence, i.e. along the $y$-direction. Note that these configurations are generally not 'longitudinal' or 'transverse' with respect to the magnetization, except for a large enough field (2 kOe) which always orients the magnetization along its own direction.

The Pt/Co/Pt film was deposited on an $Al_2O_3(0001)$ substrate. The first 5 nm thick Pt(111) buffer layer allowed initiation of the growth of an ultrathin hcp Co(0001) layer. Co layers 40 nm (20 ML) and 80 nm (40 ML) thick with small (111)-textured crystallites about 10 nm in size were slowly evaporated at 100 °C. The Co layers are finally protected by a 3 nm thick Pt top layer. The Co layer thickness is chosen in order to get the magnetization confined in the film plane. This was realized, but a weak uniaxial in-plane magnetic anisotropy is revealed by MOKE magnetometry and microscopy. The magnetic shape anisotropy of the sample is not large enough to explain the results. So, the origin of this magnetic anisotropy probably lies in the preparation conditions for the Pt/Co/Pt films. Such uniaxial anisotropy can be induced by a small miscut orientation of the sapphire substrate or by strains during the growing process.

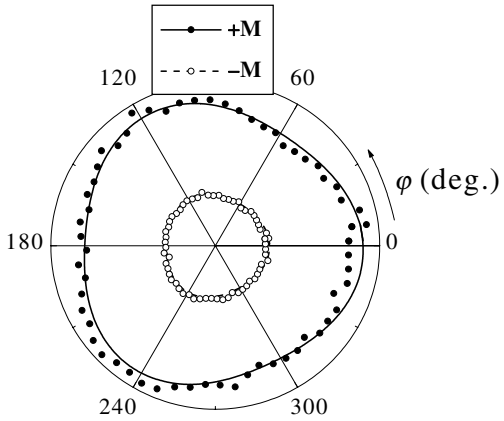


**Figure 3.** Rotational anisotropy of the MSHG in Pt/Co(20 ML)/Pt in the transverse geometry.

## 3. Experimental results and discussion

### *3.1. Rotational anisotropy and polarization dependence of SHG*

Since the Pt/Co/Pt thin films were grown on sapphire (0001), the SHG intensity should reflect the symmetry of the (0001) crystallographic plane. In order to check the induced optical anisotropy and separate the crystallographic and magnetic contributions to the SHG, rotational anisotropy measurements were first performed. In the experiments a saturating magnetic field (2 kOe) was applied along the $y$-direction (figure 2) (transverse configuration) during the experiment. Measurements were performed for two opposite orientations (+ or −) of the magnetic field. The azimuthal variation of the SHG intensity generated by the Pt/Co(20 ML)/Pt film was recorded as a function of the angle of rotation $\varphi$ around the $z$-axis (measured from the $x$-axis—see figure 2). The results are collected in figure 3, for incoming P-polarized light at the fundamental frequency and P-polarized detected SHG. The SHG signals are slightly anisotropic with a threefold anisotropy. A strong magnetic SHG contrast (or MSHG) $\rho$, up to 50%, can be measured:

$$\rho = \frac{I(2\omega, +M) - I(2\omega, -M)}{I(2\omega, +M) + I(2\omega, -M)}. \tag{4}$$

Since the Pt buffer layer is deposited on sapphire (0001), one expects a $3m$ crystallographic symmetry for the $Pt/Al_2O_3$ interface. Thus, the reflected SHG intensity obviously displays the same anisotropic property. On the other hand, magnetic Pt/Co interfaces can show either isotropic or $6mm$ symmetry, due to the preferred orientation of the hcp Co crystallites along one of the [0001] axes. The proper non-linear polarizations of SHG at oblique incidence on anisotropic interfaces having $3m$ or $6mm$ symmetry have been determined in reference [15]. The experimental data shown in figure 3 can be easily fitted using the following expression:

$$I(2\omega) = (A\cos 3\varphi + B)^2 \tag{5}$$

where the coefficients $A$ and $B$ characterize the anisotropic and isotropic contributions to the SHG intensity, respectively. Note that the anisotropic contribution has a purely crystallographic origin, whereas the isotropic one can be either crystallographically or magnetically induced. This follows from symmetry considerations of the light reflected by the anisotropic interfaces [15].

Figure 4(a) shows the longitudinal SHG signal ($\boldsymbol{M} \parallel \boldsymbol{x}$), given by the Pt/Co(20 ML)/Pt film, as a function of the azimuthal orientation $\alpha$ of the analyser with respect to the polarizer and for P-polarized fundamental light. A saturating magnetic field (2 kOe) was always applied along the $x$-axis. The MSHG contrast $\rho$ deduced using equation (4) is plotted in figure 4(b) as points.

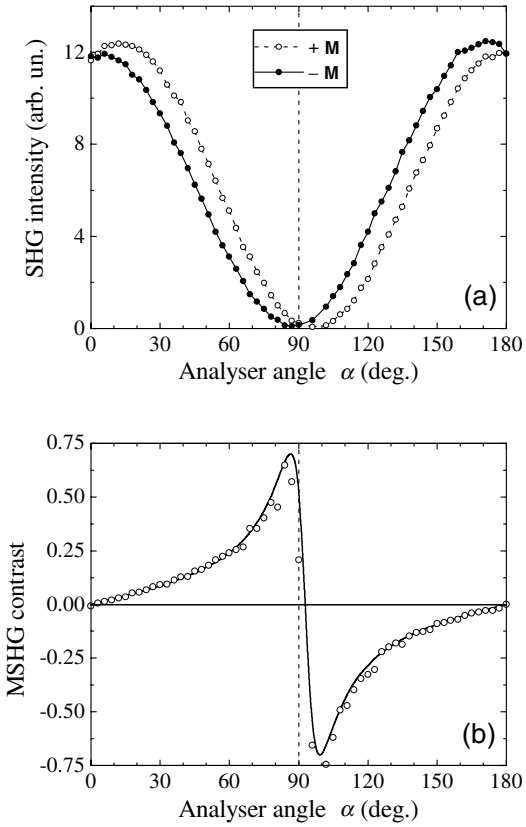


**Figure 4.** SHG intensity (a) and SHG contrast (b) for the Pt/Co(20 ML)/Pt film in the longitudinal geometry as a function of the analyser azimuthal angle $\alpha$ relative to the polarizer orientation. Dashed lines show the extinction position. The fitting parameters for the solid curve in (b) were obtained using equation (7): $\delta = -45(2)^\circ$, $\Phi = 0.111(5)$ and $\Psi = 0.050(6)$.

In the case of non-magnetic interfaces with $3m$ symmetry, one should expect both P- and S-polarized SHG emerging light for a P-polarized fundamental wave when the crystallographic and laboratory $z$-axes are parallel to each other, whatever the orientation of the crystal $x$-axis (see figure 2). For an interface having $6mm$ symmetry, the magnetization-induced SHG is S-polarized while the non-magnetic SHG is P-polarized in the longitudinal geometry [15]. The resulting SHG intensity can be written as

$$I(2\omega, \pm M) \propto \left| E^P(2\omega)\cos\alpha + E^S(2\omega)\sin\alpha \pm E^S(2\omega, \pm M)\sin\alpha \exp(\mathrm{i}\delta) \right|^2 \tag{6}$$

where $E^{P,S}(2\omega)$ are the electric field components of the SHG. Using equations (4) and (6), one gets the azimuthal dependence of the SHG contrast:

$$\rho = \frac{2\Phi\cos\delta\tan\alpha(1 + \Psi\tan\alpha)}{1 + 2\Psi\tan\alpha + (\Phi\tan\alpha)^2 + (\Psi\tan\alpha)^2} \tag{7}$$

where $\delta$ is optical phase shift and $\Phi = E^S(2\omega, M)/E^P(2\omega)$ is the ratio between the magnetic and crystallographic contributions to the optical electric field. $\Psi = E^S(2\omega)/E^P(2\omega)$ is the ratio between the S and P non-magnetic components of the optical electric field. Contrary to the isotropic case discussed in reference [16], the SHG contrast can be asymmetric for anisotropic interfaces. A maximum SHG contrast, up to 70%, was measured for $\alpha \simeq 86^\circ$ and $99^\circ$.

### *3.2. Comparison between MOKE and MSHG hysteresis loops*

The two complementary MOKE and MSHG measurements were performed here in the longitudinal configuration with the same set-up and on the same sample area. To get a good signal-to-noise ratio, the measurements using P-polarized incident light were carried out with an analyser azimuthal angle $\alpha$ of $85^\circ$ for the MOKE and $45^\circ$ for the MSHG measurements. It was difficult to perform MSHG measurements at angles corresponding to the maximum value of the contrast because of the rather low SHG intensity. Figure 5(a) shows normalized longitudinal MOKE and MSHG hysteresis loops measured in a magnetic field applied along

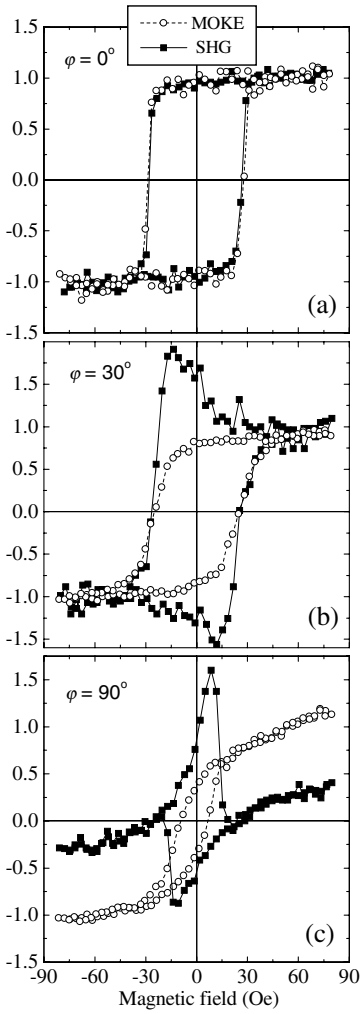


**Figure 5.** Normalized hysteresis loops measured using the MOKE and MSHG.

the easy anisotropy axis. These loops display exactly the same shape and coercivity. After rotation of the sample around of the $z$-axis by an angle $\varphi = 30^\circ$ (figure 2), which means that the high-field-induced magnetization lies at $30^\circ$ from the easy anisotropy axis, the MOKE and MSHG hysteresis loops for the same sample region lead to the same coercive field but they exhibit different shapes (figure 5(b)). Figure 5(c) shows MOKE and MSHG hysteresis loops in a magnetic field applied along the hard axis ($\varphi = 90^\circ$). As expected, the remanent MOKE signal magnetization is far smaller than that corresponding to the saturated state. The MSHG hysteresis loop shows an asymmetric shape with a higher coercivity than the MOKE loop and a remanent value larger than the saturated one (figures 5(b) and 5(c)).

In order to understand the shapes of the MSHG loops, we have to consider the field-induced magnetic behaviour of such samples with uniaxial in-plane anisotropy which may be deduced from MOKE measurements. At saturation, in large enough fields (2 kOe) and for all values of $\varphi$, MOKE microscopy proves unambiguously that one always obtains a single-domain state with magnetization parallel to the direction of the applied magnetic field. Then, if the field is switched off to zero, a non-uniform ribbon-like domain structure is observed when the field is not rigorously applied along the easy anisotropy axis $\boldsymbol{a}$, the magnetization in successive stripes being oriented alternately along the two orientations of $\boldsymbol{a}$. In this way the charges on the walls are minimized [17]. One obtains a compensated ribbon-like remnant domain structure with a period of about 2 $\mu$m only if the field is first applied exactly along the hard axis. The relative size of the plus or minus stripe domains in zero field obviously depends on the orientation of the premagnetizing field, i.e. on the value of $\varphi$. When $\varphi$ differs significantly from $90^\circ$, if one starts from the high-field saturated magnetic state, on reducing the field the magnetization begins to rotate uniformly away from the $\boldsymbol{H}$-direction towards the most stable orientation of the magnetization along the easy axis $\boldsymbol{a}$. Then, if the field is inverted and increased further, magnetization reversal takes place when the projection field along the opposite $\boldsymbol{a}$-orientation is large enough. This switching field has consequently nothing to do with the coercive field obtained in longitudinal MOKE measurements or measured when $\boldsymbol{H} \parallel \boldsymbol{a}$.

Thus, the observed magneto-optical hysteresis loops are consistent with the following model. Simulated loops involving the expected MSHG contributions are depicted in figure 6. Figure 6(a) shows the longitudinal MOKE loop when the direction of the applied magnetic field makes an angle $\varphi$ with the easy anisotropy axis. The simulated transverse contribution to the SHG (figure 6(b)) leads to a MSHG hysteresis loop with the shape depicted in figure 6(c). One must also remember that the SHG intensity has an additional contribution proportional to $M^2$ (see equation (3)). Adding the simulated contribution $M^2$ (figure 6(d)) gives rise finally to a MSHG hysteresis loop whose shape is given in figure 6(e). Thus the MSHG hysteresis loop becomes asymmetric, which is in very good agreement with the experimental data (see figure 5). In conclusion, to find the shape of the MSHG hysteresis loop shown in figure 5(c), one has to add up a linear transverse contribution with negative sign (figure 6(b)) and a transverse contribution varying as $M^2$ (figure 6(d)). Thus, the presence of an in-plane easy-axis magnetic anisotropy explains well the very different shapes of hysteresis loops measured using the MOKE or MSHG.

### *3.3. MOKE and MSHG imaging*

Both longitudinal MOKE and MSHG microscopy observations were performed on Pt/Co/Pt films with a premagnetizing field applied along the easy anisotropy axis, i.e. along the $x$-direction (figure 2). High-contrast images were obtained for the analyser azimuthal angle $\alpha = 84^\circ$. In spite of a large transverse MSHG effect, we chose to work in the longitudinal configuration since the transverse MOKE effect is rather weak [7].

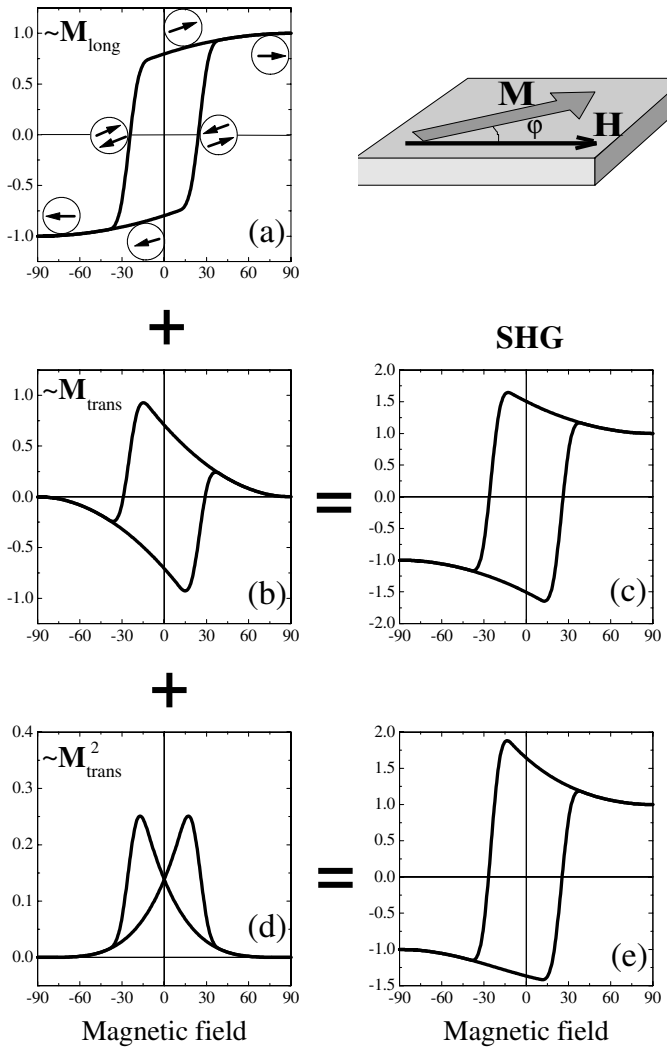


**Figure 6.** Simulated hysteresis loops for different contributions to the SHG (see the explanation in the text) and a schematic view of the magnetized sample. The corresponding hysteresis loop shapes are indicated in (c) and (e) where linear and (linear + quadratic) transverse terms are added respectively to the longitudinal contribution. In (a) the arrows indicate the spin orientation, if one supposes that the abscissa axis is the $x$-direction and the ordinate axis is the $y$-direction.

For the MOKE imaging we used the following procedure. A reference remnant ($H = 0$) image was first recorded after saturating the film in a large enough premagnetizing field; then a second remnant ($H = 0$) image of the magnetic pattern, obtained after applying a reversed field $\boldsymbol{H}$, was subtracted by image processing from the reference. The field-induced states are then frozen after switching off the applied field to zero before carrying out the image acquisitions. This procedure allows one to avoid stray field-induced Faraday effects in the optical elements. The longitudinal MOKE and MSHG images of the magnetic domain structure for the same sample area are reported in figure 7 for the Pt/Co(20 ML)/Pt and Pt/Co(40 ML)/Pt films. Due to the large angle of light incidence (45°) on the film (figure 2), the contrast of the MSHG images

decreases rapidly outside the depth of focus, i.e. the intensity can be considered as nearly homogeneous over a short lateral distance (along the $x$-direction) of no more than 30 $\mu$m. This was the main limitation of previous MSHG domain observations on CoNi/Pt films [7]. Therefore a sample scanning procedure was applied here to investigate larger areas. Due to the very low non-linear optical efficiency, it was necessary to take an exposure time of ten minutes for each MSHG image over a reduced sample area about 30 $\mu$m in diameter. Using stepper motors, the sample was scanned along the $x$- and $y$-directions and thus imaging was performed on many neighbouring areas of the sample. MSHG images were then constructed from 81 small single images (figures 7(b), 7(d)). The magnetic image resolution is estimated here to be about 2 $\mu$m.

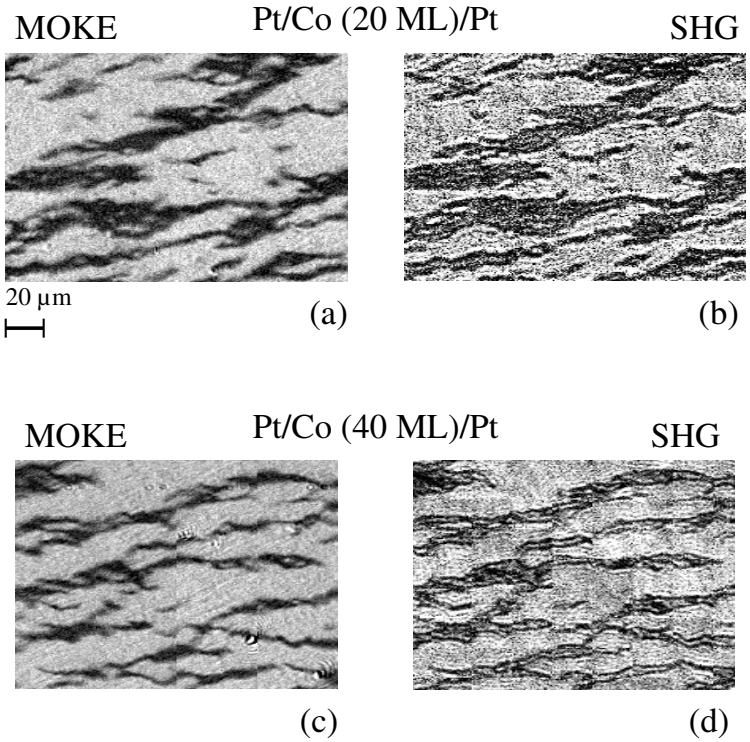


**Figure 7.** MOKE and MSHG images for Pt/Co(20 ML)/Pt ((a), (b)), and for Pt/Co(40 ML)/Pt films ((c), (d)). The field was previously applied along the easy anisotropy axis set parallel to $\boldsymbol{x}$ (see figure 1).

Due to the larger field of view of the MOKE microscopy set-up, each MOKE image resulted only from the accumulation of ten images acquired during two seconds each. The MOKE patterns were built up from four images scanned in the $x$-direction.

It is clear that MOKE and MSHG images show very similar domain patterns for both Co thicknesses of 20 and 40 ML. In the MOKE image each domain has the same shape and position as its counterpart in MSHG microscopy. It is reasonable to observe close domain patterns at the Pt/Co interfaces and inside the Co layer since the Co film thickness (4 or 8 nm) does not exceed the magnetic exchange coherence length for Co (4 nm) much. Therefore the domain formation inside the Co layer is necessarily strongly coupled to the magnetization state at the Pt/Co interfaces. However, in domain wall regions an additional contrast can be visualized in

MSHG images at domain wall boundaries (figure 7). It is well known that for films with weak in-plane anisotropy, 180° symmetric Néel walls spread very much [17]. Using the measured value for the anisotropy and a usual assessment of the exchange stiffness, we deduced a domain wall width of about 100 nm in this case. At such low Co layer thicknesses, closure domains are unfavourable. The fact that transverse contributions to the MSHG response are important for this sample explains well the observed enhancement of the contrast in domain wall regions, where the mean magnetization is perpendicular to the plane of incidence of the light ($\|\boldsymbol{y}$). An additional explanation of such fine structure at wall boundaries could be the existence of a MSHG contribution proportional to the magnetization gradient [18].

Thus, we have implemented a combined experimental technique for the observation of linear and non-linear magneto-optical images. Experiments in the longitudinal configuration have shown that it was possible to get MO images with high contrast in MOKE and in SHG microscopy. The longitudinal configuration is here more suitable than the transverse geometry for comparing linear and non-linear MO effects [7].

## 4. Conclusions

Pt/Co/Pt films with in-plane magnetic anisotropy have been studied by means of two complementary magneto-optical methods. MOKE measurements probe the magnetization over the whole thickness of the thin Co magnetic film whereas the MSHG is only sensitive to the state of magnetization at the surface and interfaces. Large magnetic MSHG contrasts, up to 50% in the transverse geometry and up to 70% in the longitudinal configuration, have been obtained. The longitudinal MOKE and MSHG hysteresis loops can have different shapes when the field is not applied rigorously parallel to the easy in-plane anisotropy axis. As expected, since the Co film thickness is comparable to the exchange coherence length, MOKE and MSHG microscopy images of the same sample area reveal quite similar magnetic domain structures. Nevertheless, the MSHG image shows additional structures at wall boundaries. The difference between MOKE and MSHG images is well explained by the presence of transverse MSHG contributions in the longitudinal geometry used for the measurements.

## Acknowledgments

We wish to acknowledge Laurent Belliard who obtained and analysed the first MOKE microscopy data on similar Co/Pt samples. Part of this work was supported by INTAS and the European TMR (NOMOKE) network. VVP acknowledges the financial support of the CNRS through an associated scientist position at the Paris-Sud University and the Russian Foundation for Basic Research.

## References

[1] Carcia P F 1987 *J. Vac. Sci. Technol.* **5** 1975
[2] Zeper W B, Greidanus F J A M, Carcia P F and Fincher C R 1989 *J. Appl. Phys.* **65** 4974
[3] Lee C H, Farrow R F C, Lin C J, Marienero E E and Chien C J 1990 *Phys. Rev.* B **42** 11 384
[4] Bennemann K H (ed) 1998 *Nonlinear Optics in Metals* (Oxford: Oxford University Press)
[5] Kurimura S and Uesu Y 1997 *J. Appl. Phys.* **81** 369
[6] Kirilyuk A, Kirilyuk V and Rasing Th 1997 *Appl. Phys. Lett.* **70** 2306
[7] Kirilyuk A, Kirilyuk V and Rasing Th 1999 *J. Magn. Magn. Mater.* **198+199** 620
[8] Smolyaninov I I, Zayats A V and Davis C C 1997 *Opt. Lett.* **22** 1592
[9] Wegner D, Conrad U, Güdde J, Meyer G, Crecelius T and Bauer A 2000 *J. Appl. Phys.* **88** 2166

[10] Fiebig M, Fröhlich D, Kohn K, Leute St, Lottermoser Th, Pavlov V V and Pisarev R V 2000 *Phys. Rev. Lett.* **84** 5620
[11] Train C and Mathet V 1998 *Surf. Sci.* **412+413** 495
[12] Shen Y R 1984 *The Principles of Nonlinear Optics* (New York: Wiley)
[13] Tessier G, Malouin C, Georges P, Brun A, Renard D, Pavlov V V, Meyer P, Ferré J and Beauvillain P 1999 *Appl. Phys.* B **68** 545
[14] Belotelov V I, Pyatakov A P, Eremin S A, Musaev G G and Zvezdin A K 2000 *Phys. Solid State* **42** 1873
[15] Banshchikov A G, Kimel A V, Pavlov V V, Pisarev R V, Sokolov N S and Rasing Th 2000 *Phys. Solid State* **42** 909
[16] Straub M, Vollmer R and Kirschner J 1996 *Phys. Rev. Lett.* **77** 743
[17] Hubert A and Schäfer R 1998 *Magnetic Domains: the Analysis of Magnetic Microstructures* (Berlin: Springer)
[18] Petukhov A V, Lyubchanskii I L and Rasing Th 1997 *Phys. Rev.* B **56** 2680